Cellular & Molecular Biology Letters

RESEARCH ARTICLE

Open Access

IL-6-induced long noncoding RNA MIR3142HG promotes tumorigenesis by interacting with thioredoxin-1 and STAT3 in human colorectal cancer

Daoquan Fang[1†], Qian Feng[2,3,4†], Baojian Zhou[1†], Yangyang Liu[1†], Yichu Lian[1], Yihui Zhang[5], Dichen Yang[1], Xintong Liu[1], Xiaomeng Shi[1], Wuhua Ni[5*] and Lei Jiang[1,6*]

†Daoquan Fang, Qian Feng, Baojian Zhou, and Yangyang Liu have contributed equally to this work.

*Correspondence:
niwuhua228@163.com; lei.jiang@wmu.edu.cn

[1] Central Laboratory, the First Affiliated Hospital of Wenzhou Medical University, Wenzhou 325000, China
[2] Department of Gastroenterology, Affiliated Hangzhou First People's Hospital, Westlake University School of Medicine, Hangzhou, Zhejiang, China
[3] Key Laboratory of Integrated Traditional Chinese and Western Medicine for Biliary and Pancreatic Diseases of Zhejiang Province, Hangzhou, Zhejiang, China
[4] Hangzhou Institute of Digestive Diseases, Hangzhou, Zhejiang, China
[5] Reproductive Medicine Center, the First Affiliated Hospital of Wenzhou Medical University, Wenzhou 325000, China
[6] Zhejiang Key Laboratory of Intelligent Cancer Biomarker Discovery and Translation, First Affiliated Hospital, Wenzhou Medical University, Wenzhou 325035, China

Abstract

Background: Colorectal cancer (CRC) is a prevalent and highly malignant neoplasm on a global scale, ranking as the second most widespread cause of cancer-associated death. Long noncoding RNAs (lncRNAs) control tumorigenic processes in CRC by modulating inflammatory signals. However, the precise mechanisms remain unknown.

Methods: LncRNAs regulated by thioredoxin-1 (Trx-1) and interleukin (IL)-6 were identified by RNA sequencing (RNA-seq). The effect of MIR3142HG on CRC growth, migration, and invasion was assessed through methods of cell counting kit-8 (CCK-8), colony formation assay, Transwell assay, and animal experimentation, respectively. The regulation of signal transducer and activator of transcription 3 (STAT3) on the MIR3142HG promoter was verified using chromatin immunoprecipitation (ChIP) and dual-luciferase reporter assays. The interaction of MIR3142HG with Trx-1 and STAT3 proteins was validated with RNA-binding protein immunoprecipitation (RIP) and RNA-pulldown experiments. Bioinformatics analysis and tissue microarray were utilized for evaluating the clinical value of MIR3142HG in CRC.

Results: We identified a lncRNA, MIR3142HG, regulated by Trx-1 knockdown and IL-6 treatment. Overexpression of MIR3142HG enhanced CRC cell proliferation, migration, and invasion, while its knockdown impaired these processes. STAT3 bound to the MIR3142HG promoter and activated its transcription. Upregulated MIR3142HG acted as a scaffold for the Trx-1/STAT3 complex to inhibit the degradation of Trx-1 and phosphorylated STAT3 (p-STAT3). In situ hybridization (ISH) results of CRC tissues indicated that MIR3142HG expression was significantly elevated during the early stages of CRC. Moreover, consistent with the Cancer Genome Atlas (TCGA) dataset, high MIR3142HG expression predicted better survival.

Conclusions: Our study identified a novel lncRNA MIR3142HG, which interacts with STAT3 and Trx-1 to promote CRC progression, providing a possible diagnostic target for CRC.

Keywords: MIR3142HG, IL-6, STAT3, Trx-1, CRC

Graphical Abstract
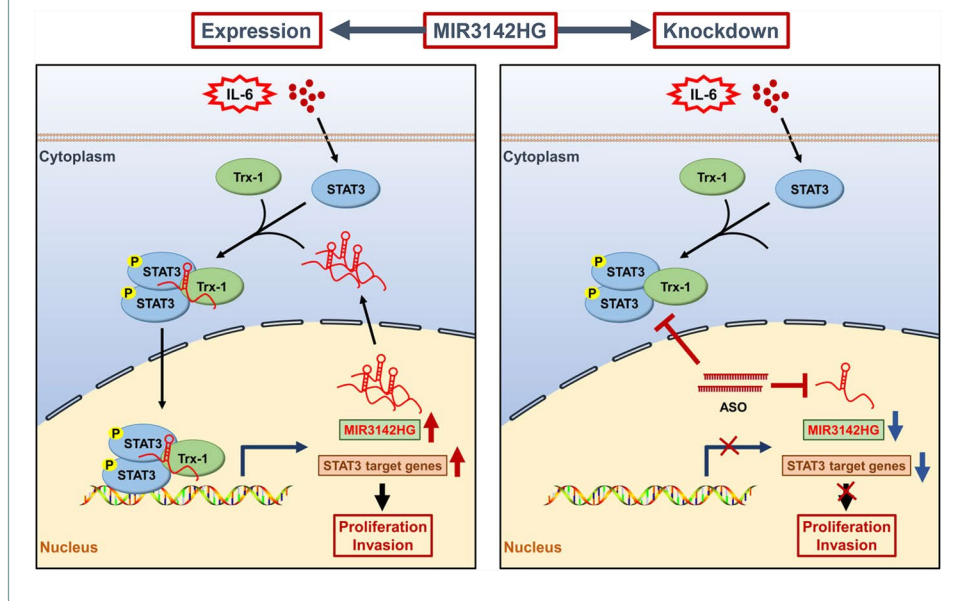
Background

Colorectal cancer (CRC) is the third most common malignancy worldwide and the second leading cause of cancer-related death [1, 2]. Chronic inflammation is thought to promote tumorigenesis and the development of CRC [3, 4]. Interleukin (IL)−6, a crucial inflammatory factor, is abnormally elevated in the tumor microenvironment owing to chronic inflammation and plays an important role in tumorigenesis and cancer progression [5–7]. IL-6 activates the downstream transcription factor signal transducer and activator of transcription 3 (STAT3), causing it to be phosphorylated and translocated into the nucleus to initiate the transcription of target genes, which promotes tumor cell growth and metastasis [8, 9]. In addition, IL-6 levels are increased in the serum and cancer tissue of patients with CRC, and its concentration is associated with tumor aggressiveness and lower survival [10, 11]. The IL-6/STAT3 pathway is a promising target. However, targeting the IL-6/STAT3 signaling pathway requires a better understanding of the specific downstream effectors.

Long noncoding RNAs (lncRNAs) are a cluster of RNAs that are more than 200 nucleotides long and have no protein-coding potential, with the exception of those that can produce functional small peptides [12]. There is increasing evidence that disturbance of lncRNA expression may be a pathogenic event in many diseases, including cancer [13]. In addition to the classical IL-6/STAT3 signaling axis, it has been reported that IL-6 can induce the expression of lncRNAs to promote tumor progression [14]. A study showed that a positive feedback loop between lnc-UICC and the IL-6/STAT3 signaling pathway drives cervical cancer progression by enhancing tumor growth and metastasis [15]. In another study, a novel lncRNA, AU021063, induced by IL-6/Arid5a signaling, was found to promote breast cancer metastasis by stabilizing Trib3 and activating the Mek/Erk pathway [14]. The role of lncRNAs in regulating the IL-6/STAT3 signaling pathway has also been extensively studied. The lncRNA LEISA promotes the binding of STAT3 to the

Fang *et al. Cellular & Molecular Biology Letters*   (2025) 30:61

Page 3 of 19

IL-6 promoter, leading to increased proliferation and decreased apoptosis of lung adeno-carcinoma cells [16]. Another study demonstrated that lncRNA XIST promotes breast cancer stem cell properties by activating the IL-6/STAT3 signaling pathway [17].

Thioredoxin-1 (Trx-1) is a small redox protein that plays a key role in cancer progression [18, 19]. Trx-1 protects tumor cells through antioxidative, antiapoptotic, and antiinflammatory effects under various stress conditions [19, 20]. Our previous study revealed that IL-6-induced Trx-1 nuclear translocation plays a key role in CRC development by activating the IL-6/STAT3 signaling axis through interaction with STAT3 [21]. However, it is unclear whether lncRNAs are involved in this molecular process. In this study, we identified a novel lncRNA regulated by IL-6, MIR3142HG, which promotes CRC progression by activating the IL-6/STAT3 signaling pathway through its interaction with STAT3 and Trx-1.

Methods

Cell culture

Human CRC cell lines SW480 (SCSP-5033), HT-29 (SCSP-5032), DLD-1 (SCSP-5241), SW620 (TCHu101), and the HEK-293 T (SCSP-502) cell line were purchased from the Cell Bank of the Chinese Academy of Sciences (Shanghai, China). All cell lines were subjected to short tandem repeat (STR) analysis and mycoplasma testing. SW480 cells were cultured in Leibovitz's L-15 Medium (Gibco, Grand Island, NY, USA) supplemented with 10% fetal bovine serum (FBS) (Sigma–Aldrich, St. Louis, MO, USA). HT-29, DLD-1, and SW620 cells were cultured in RPMI 1640 Medium (Gibco, Grand Island, NY, USA) supplemented with 10% FBS. HEK293 T cells were cultured in Dulbecco's modified Eagle's medium (DMEM, Gibco, Grand Island, NY, USA) supplemented with 10% FBS. The cells were incubated at 37 °C in a humidified atmosphere with 5% CO_2. Recombinant human IL-6 was purchased from R&D Systems (Minneapolis, MN, USA) and reconstituted at a concentration of 100 μg/mL in sterile phosphate-buffered saline (PBS) supplemented with 0.1% bovine serum albumin (BSA).

Transfection with antisense oligonucleotide (ASO) and small interfering RNA (siRNA)

The design and synthesis of ASOs targeting MIR3142HG were performed by RiboBio (Guangzhou, China). SiRNA targeting STAT3 was synthesized by GenePharma (Suzhou, China). Lipofectamine 3000 (Invitrogen, Carlsbad, CA, USA) was used to transfect the cells with siRNA or ASOs. Supplementary Material Table S1 lists the sequences of the siRNAs and ASOs.

Plasmid construction

The full-length cDNA of MIR3142HG was amplified and subsequently cloned and inserted into the lentiviral expression vector pCDH-EF1-MCS-BGH-PGK-copGFP-T2 A-Puro (System Biosciences, USA). Cotransfection of the lentiviral packaging plasmids pMD2. G, pMDL-G/P-RRE, and pRSV-REV were performed with pCDH-MIR3142HG in HEK-293 T cells. The lentiviruses were harvested after 48 h of incubation. To generate stable transfectants, CRC cell lines were infected with lentivirus and then subjected to selection with 2 μg/mL puromycin for 2 weeks. Lentiviral vectors containing shRNAs

targeting Trx-1 or the luciferase gene were previously constructed in our lab [22]. The sequences of shTrx-1 and shLuc are listed in Supplementary Material Table S1.

Cell proliferation assay

CRC cells were seeded in 96-well plates at a density of 3×10^3 cells/well and then incubated at 37 °C in a CO_2 incubator. Cell viability was assessed at 24 h intervals. In each well, 10 μL of cell counting kit-8 (CCK-8) solution (Dojindo, Kumamoto, Japan) was added, followed by incubation at 37 °C for 3 h and measurement of the cell absorbance at 450 nm.

Colony formation assay

After the cells were seeded into six-well plates at a density of 1×10^3 cells/well, the plates were incubated at 37 °C in a 5% CO_2 incubator. After 2 weeks, the cells were fixed with 4% paraformaldehyde and stained with 0.1% crystal violet. After extensive washing and air drying, the plates were photographed. ImageJ software (NIH, Washington, DC, USA) was used to quantify the colonies.

Transwell assay

The assay for cell migration and invasion was performed using 8-μm Transwell cell culture chamber filters (Corning, Cambridge, MA, USA). Prior to the invasion assay, the chamber membranes were precoated with Matrigel. After the cells were suspended in serum-free medium at a concentration of 5×10^4 cells/mL, they were cultured in the upper chamber, while the lower chamber was filled with medium containing 20% FBS. After 36–48 h, the cells were fixed with 4% paraformaldehyde and stained with 0.1% crystal violet. The cells in the upper chamber were then removed, and the remaining cells were photographed via an inverted microscope (CKX53, Olympus, Japan). The number of cells was quantified via ImageJ software.

Western blot analysis

The cells were lysed with radioimmunoprecipitation assay buffer (RIPA) Lysis and Extraction Buffer (Thermo Fisher Scientific, Waltham, MA, USA) supplemented with protease and phosphatase inhibitors (Thermo Fisher Scientific) to obtain total protein, while the nuclear and cytoplasmic fractions were prepared with NE-PER Nuclear and Cytoplasmic Extraction Reagents (Thermo Fisher Scientific). Proteins of equal mass from each sample were separated via sodium dodecyl sulfate (SDS)–polyacrylamide gel electrophoresis and electrotransferred to a polyvinylidene difluoride membrane (Millipore, Billerica, MA, USA). The membranes were then blocked in 5% skim milk for at least 2 h at RT. The membranes were then incubated with primary antibodies overnight at 4 °C and with secondary antibodies labeled with horseradish peroxidase for 1 h at RT. Primary antibodies against glyceraldehyde-3-phosphate dehydrogenase (GAPDH; no. ET1601-4, 1:10000, HUABIO, China), histone H3 (no. VPA00826, 1:1000, Bio-Rad, California, CA, USA), Trx-1 (no. ab133524, 1:10000, Abcam, Cambridge, MA, USA), E-cadherin (no. 3195, 1:1000, Cell Signaling Technology, Danvers, MA, USA), vimentin (no. 5741, 1:1000, Cell Signaling Technology), STAT3 (no. 4904, 1:2000, Cell Signaling Technology), and phosphorylated STAT3 (p-STAT3; Tyr705) (no. 9145, 1:2000, Cell Signaling

Technology) were used. The specific bands were detected via an enhanced chemiluminescence detection system (Bio-Rad).

Quantitative reverse transcription polymerase chain reaction (qRT-PCR)

TRIzol (Thermo Fisher Scientific) was used to extract total RNA from cells and tissues. Total RNA was then reverse transcribed with PrimeScript™ RT Master Mix (Takara, Kusatsu, Japan). For qRT-PCR, TB Green™ Premix Ex Taq™ II (Takara) was used to quantify the expression of lncRNAs or mRNAs according to the manufacturer's instructions via the QuantStudio 5 real-time PCR system (Applied Biosystems, Warrington, UK). The endogenous control GAPDH was used to normalize the expression of lncRNAs or mRNAs. The separation of cytoplasmic and nuclear RNA was performed via a PARIS Kit (Thermo Fisher Scientific, Waltham, MA, USA) according to the manufacturer's protocols. A qRT-PCR assay was subsequently used to detect the expression of MIR3142HG in the cytoplasm and nucleus. The results were normalized to those of GAPDH and U6. The $2^{-\Delta\Delta CT}$ method was used to calculate the relative expression. All specific PCR and RT primer sequences are listed in Supplementary Material Table S2.

Organoid culture and ASOs treatment

Coloctal cancer tissue was obtained from surgical resection specimens. The tissue samples were minced and digested for approximately 30 min until no obvious tissue clumps were present. The samples were filtered through a 100 μm filter and washed with basal medium. The cells were then plated in a 24-well cell culture plate at a density of 1×10^4 cells per 50 μL of Matrigel (Corning, Cambridge, MA, USA) at the bottom of each well. After the Matrigel solidified, 500 μL of complete colorectal cancer organoid culture medium (Xiamen Mogengel, China) was added to each well. For ASOs treatment, organoids were seeded in a 96-well plate, and ASOs were added under sterile conditions to reach a final concentration of 5 μM per well. The organoids were incubated in a cell culture incubator at 37 °C with 5% CO_2. During the incubation period, the growth status of the organoids was continuously observed. After 3 days, the medium was changed, and the ASOs were replenished. Organoid viability was determined via CellTiter-Glo® 2.0 (Promega, Madison, WI, USA) by quantifying adenosine triphosphate (ATP) production 5 days after treatment. This study was approved by the Ethics Committee of the First Affiliated Hospital of Wenzhou Medical University.

Tumor xenograft model

The animal experiment protocol was approved by the Laboratory Animal Ethics Committee of the First Affiliated Hospital of Wenzhou Medical University; 4-week-old male athymic BALB/c nude mice were purchased from Shanghai SLAC Laboratory Animal Co. Ltd. (Shanghai, China). Approximately 5×10^6 SW480 cells were administered subcutaneously into the right flank of male BALB/c nude mice. Tumor size was determined via a Vernier caliper, and intratumoral injections of NC-ASO or MIR3142HG-ASO (5 nmol/injection) were administered every 3 days ($n = 5$ per treatment group). After the mice were euthanized, the subcutaneous tumors were dissected and subsequently weighed. The tumor volume was calculated via the following formula: $V = 0.5 \times D \times d^2$ (V, volume; D, longest diameter; d, diameter perpendicular to the longest diameter).

Immunohistochemistry

The expression of p-STAT3 and proliferation marker protein Ki-67 (Ki-67) in the tumors was characterized via immunohistochemistry with specific antibodies. The tumor tissue was fixed and then embedded in paraffin for sectioning. Antigenic sites that may have been masked during the fixation process were uncovered via antigen retrieval methods. The sections were incubated with an anti-Ki-67 antibody (no. ab16667, 1:250, Abcam, Cambridge, MA, USA) and an anti-p-STAT3 antibody (no. 9145, 1:200, Cell Signaling Technology, Danvers, MA, USA) at 4 °C overnight. After washing, secondary antibodies were applied, and the samples were incubated with the primary antibodies for 2 h at room temperature. After visualization with 3,3′-diaminobenzidine, the expression of Ki-67 and p-STAT3 was assessed via a visual scoring system on the basis of the intensity of staining under a light microscope.

Dual-luciferase reporter assays

The different MIR3142HG promoter regions were subcloned and inserted into the pGL3-basic plasmid (Promega, Madison, WI, USA). The different MIR3142HG promoter reporter plasmids together with the STAT3 expression vector were transfected into HEK-293 T cells in 24-well plates at a density of 5×10^5 cells/well and cultured for 24 h. Luciferase activity was evaluated via the Dual-Luciferase Reporter Assay System (Promega, Madison, WI, USA) according to the manufacturer's guidelines. The internal control used for normalization was Renilla luciferase.

Chromatin immunoprecipitation (ChIP)

The EZ ChIP™ Chromatin Immunoprecipitation Kit (Millipore, USA) was used to perform ChIP. In brief, the cells were incubated with 1% formaldehyde at 37 °C for 10 min to cross-link histones and DNA. The cells were subsequently pelleted and resuspended in SDS lysis buffer. The lysates were sonicated on ice to shear them to lengths between 200 and 1000 bp and incubated with protein A agarose beads and an antibody against p-STAT3 (no. 9145, 1:2000, Cell Signaling Technology) overnight at 4 °C on a rotator. The combined eluates were heated at 65 °C with 5 M NaCl for 4 h to reverse the histone–DNA crosslinks. PCR analysis of the purified DNA fragments with the primers listed in Supplementary Material Table S3.

Biotin-labeled RNA pulldown assay

The full-length cDNA of MIR3142HG was inserted into the plasmid pcDNA3.1(+), which contains the T7 RNA polymerase promoter sequence. The transcription of MIR3142HG RNAs labeled with biotin was conducted in vitro via a biotin–RNA labeling mixture (Roche, Penzberg, Germany) and T7 RNA polymerase (Roche, Penzberg, Germany). The RNA was subsequently subjected to treatment with RNase-free DNase I (Promega, Madison, WI, USA). After the purification process, the biotinylated RNAs were incubated overnight at 4 °C with the cell lysate. M-280 Streptavidin magnetic beads (Invitrogen) were added to the cell lysate and then incubated for 1 h at

room temperature (RT) with rotation. Following the pulldown process, the proteins were eluted with 1× SDS loading buffer, and western blot analysis was performed.

RNA-binding protein immunoprecipitation (RIP)

The RIP assay was performed via an EZ-Magna RIP™ RNA-Binding Protein Immuno-precipitation Kit (Millipore, Billerica, MA, USA) according to the manufacturer's protocols. In brief, after thorough lysis of SW480 cells with RIP lysis buffer on ice, the RIP lysate was incubated overnight at 4 °C with RIP immunoprecipitation buffer containing magnetic beads conjugated with Trx-1 antibody (no. ab133524, Abcam, Cambridge, MA, USA) or the corresponding immunoglobulin (Ig)G (no. B900630, Proteintech, China). The coimmunoprecipitated RNAs were isolated and purified according to the kit instructions. These RNAs were subsequently subjected to reverse transcription to generate cDNA. The coimmunoprecipitated RNAs were determined via a qRT-PCR assay.

RNA fluorescence in situ hybridization (RNA-FISH)

RNA-FISH of MIR3142HG was performed via the ViewRNA® Cell Plus Assay (Thermo Fisher Scientific, Waltham, MA, USA) according to the manufacturer's instructions. The cells were fixed and permeabilized at RT for 0.5 h when they were approximately 70% confluent. After incubation of the diluted ViewRNA Cell Plus Probe with the cells for 2 h at 40 °C and four gentle washes with the ViewRNA Cell Plus RNA Wash Buffer Solution, the cells were incubated first with the preamplifier mixture, then with the amplifier mixture, and finally with the label probe mixture for 1 h each at 40 °C. ProLong™ Diamond Antifade Mountant with 4′,6-diamidino-2-phenylindole (DAPI; Thermo Fisher Scientific) was used to mount the slides.

In situ hybridization (ISH)

ISH was used to investigate the expression of MIR3142HG in CRC tissue microarrays. They included 443 paraffin-embedded tumor tissues and 59 normal tissues from a total of 443 patients with CRC at the First Affiliated Hospital of Wenzhou Medical University between 2014 and 2016. The sections were deparaffinized, digested with protease K, hydrated, and deproteinated. The MIR3142HG probes diluted with hybridization solution were carefully applied to each section, followed by incubation in a humid box at 42 °C for 24 h. After 30 min of blocking buffer, the samples were incubated with the diluted anti-DIG antibody at a constant 4 °C overnight. Prior to dehydration, counterstaining with hematoxylin was performed. This study was approved by the Ethics Committee of the First Affiliated Hospital of Wenzhou Medical University.

Statistical analysis

The experimental data are presented as the means ± standard deviations (SDs). At least three independent experiments were performed. For the statistical analyses, one-way ANOVA or two-tailed *t*-tests were performed via GraphPad Prism 8.0 (La Jolla, CA, USA) or SPSS 19.0 (Chicago, IL, USA) software. All tests were two-sided, and $P < 0.05$ was considered a significant difference.

Fang *et al. Cellular & Molecular Biology Letters*   (2025) 30:61

Page 8 of 19

Results

The expression of the lncRNA MIR3142HG is increased under IL-6 treatment in CRC cells

Our previous study revealed that the IL-6-induced nuclear translocation of Trx-1 promotes CRC development by interacting with STAT3 [21]. However, it is still unclear whether lncRNAs are involved in this process. To investigate the possible role of lncRNAs in this molecular mechanism, we performed RNA-seq to detect changes in ncRNA expression in SW480 cells stably expressing control shLuc (shRNA targeting luciferase) or shTrx-1 (shRNA targeting Trx-1) and treated them with IL-6. Western blot analysis revealed that the level of phosphorylated STAT3 protein was suppressed in SW480 cells after Trx-1 was knocked down (Fig. 1A). Three different treatments
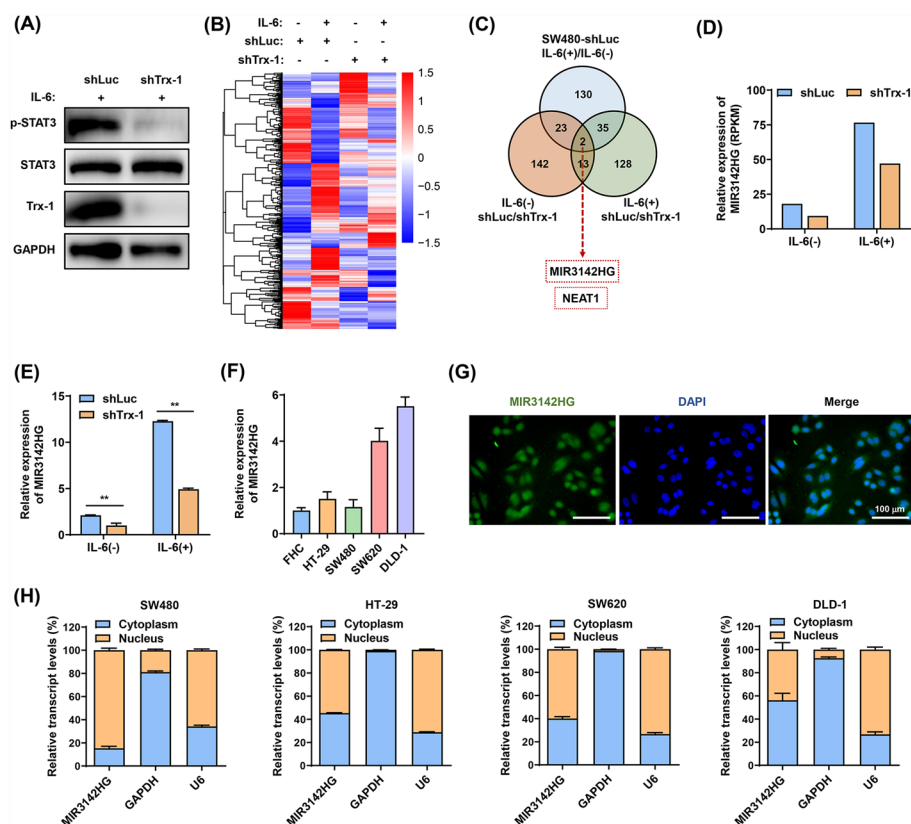
Fig. 1 The expression of the lncRNA MIR3142HG is increased under IL-6 treatment in CRC cells. **A** Protein expression of Trx-1, STAT3, and p-STAT3 in SW480 cells transfected with lenti-shTrx-1 or lenti-shLuc and treated with 20 ng/mL IL-6 for 24 h was detected by western blotting. **B** Hierarchical clustering analysis of 473 lncRNAs that were differentially expressed in SW480 cells transfected with lenti-shTrx-1 or lenti-shLuc and treated with 20 ng/mL IL-6 or vehicle control for 24 h. **C** Venn diagram of the overlapping differentially expressed lncRNAs between the three different treatments as indicated. Differentially expressed genes (including both upregulated and downregulated) were screened in the comparisons of shLuc IL-6(−) versus shLuc IL-6(+), shLuc IL-6(−) versus shTrx-1 IL-6(−), and shLuc IL-6(+) versus shTrx-1 IL-6(+) using the thresholds of |log2 FC| > 0.5 and $p < 0.05$. **D, E** The relative expression of MIR3142HG in SW480 cells transfected with lenti-shTrx-1 or lenti-shLuc and treated with 20 ng/mL IL-6 or vehicle control for 24 h was detected by RNA-seq (**D**) or qRT-PCR (**E**). **F** The relative expression of MIR3142HG in a colorectal cancer cell line and a normal colorectal epithelial cell line, FHC, was detected via qRT-PCR. **G** MIR3142HG intracellular localization in SW480 cells was visualized via RNA-FISH. Scale bar: 100 μm. **H** The subcellular localization of MIR3142HG in colorectal cancer cell lines was detected via qRT-PCR. Data represent the mean ± SD of three independent experiments. **$P < 0.01$

Fang *et al. Cellular & Molecular Biology Letters*　　(2025) 30:61

Page 9 of 19

were compared in SW480 cells: shLuc IL-6(−)/shLuc IL-6(+), shLuc IL-6(−)/shTrx-1 IL-6(−), and shLuc IL-6(+)/shTrx-1 IL-6(+) were used to screen for differential genes (Fig. 1B), where genes with $\log_2|FC| > 0.5$ and $p < 0.05$ were considered differentially expressed. The three datasets showed an overlap of two targets: MIR3142HG and NEAT1 (Fig. 1C). The mechanism of the regulation of STAT3 by NEAT1 in cancer has been previously reported [23, 24]; however, the function of MIR3142HG remains unknown. RNA-seq and qRT-PCR analyses revealed that MIR3142HG was increased in SW480 cells treated with IL-6 for 24 h and downregulated in SW480 cells with Trx-1 knockdown (Fig. 1D, E). In addition, the expression of MIR3142HG was determined in CRC cell lines (HT-29, SW480, SW620, and DLD-1) and in the normal colon epithelial cell line FHC via qRT-PCR analysis (Fig. 1F). RNA-FISH and nuclear/cytoplasmic RNA fractionation assays revealed that MIR3142HG was localized in both the nucleus and cytoplasm of the CRC cell lines; however, it was more abundant in the nucleus, as shown in Fig. 1G, H.
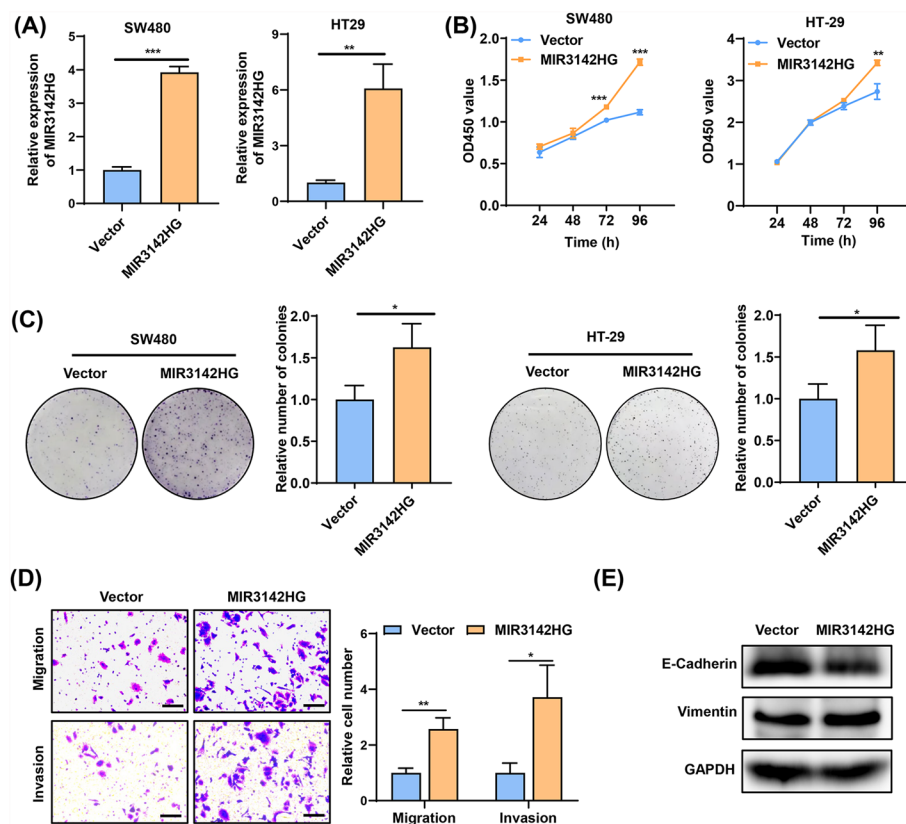

Fig. 2 MIR3142HG overexpression promotes CRC cell proliferation, migration, and invasion. **A** qRT-PCR was used to assess the effects of lentivirus-mediated ectopic overexpression of MIR3142HG in SW480 and HT-29 cells. **B**, **C** The proliferation ability of vector control or MIR3142HG-overexpressing SW480 and HT-29 cells was assessed by CCK-8 (**B**) and colony formation assays (**C**). **D** The migration and invasion abilities of vector control- and MIR3142HG-overexpressing SW480 cells were assessed via Transwell assays. Scale bar: 100 μm. **E** E-cadherin and vimentin protein expression in vector control- and MIR3142HG-overexpressing SW480 cells was detected by western blot analysis. Data represent the mean ± SD of three independent experiments. *$P < 0.05$, **$P < 0.01$, ***$P < 0.001$

MIR3142HG overexpression promotes CRC cell proliferation, migration, and invasion

SW480 and HT-29 cells stably expressing full-length MIR3142HG were constructed to investigate the function of MIR3142HG in CRC. The overexpression of MIR3142HG in SW480 and HT-29 cells was confirmed by qRT-PCR (Fig. 2A). Based on CCK-8 and colony formation assays, overexpression of MIR3142HG promoted the proliferation (Fig. 2B) and colony formation (Fig. 2C) of CRC cells. Transwell assays showed that overexpression of MIR3142HG increased CRC cell migration and invasion (Fig. 2D). Consistent with this finding, E-cadherin protein expression was reduced in MIR3142HG-overexpressing cells, whereas vimentin was upregulated (Fig. 2E).
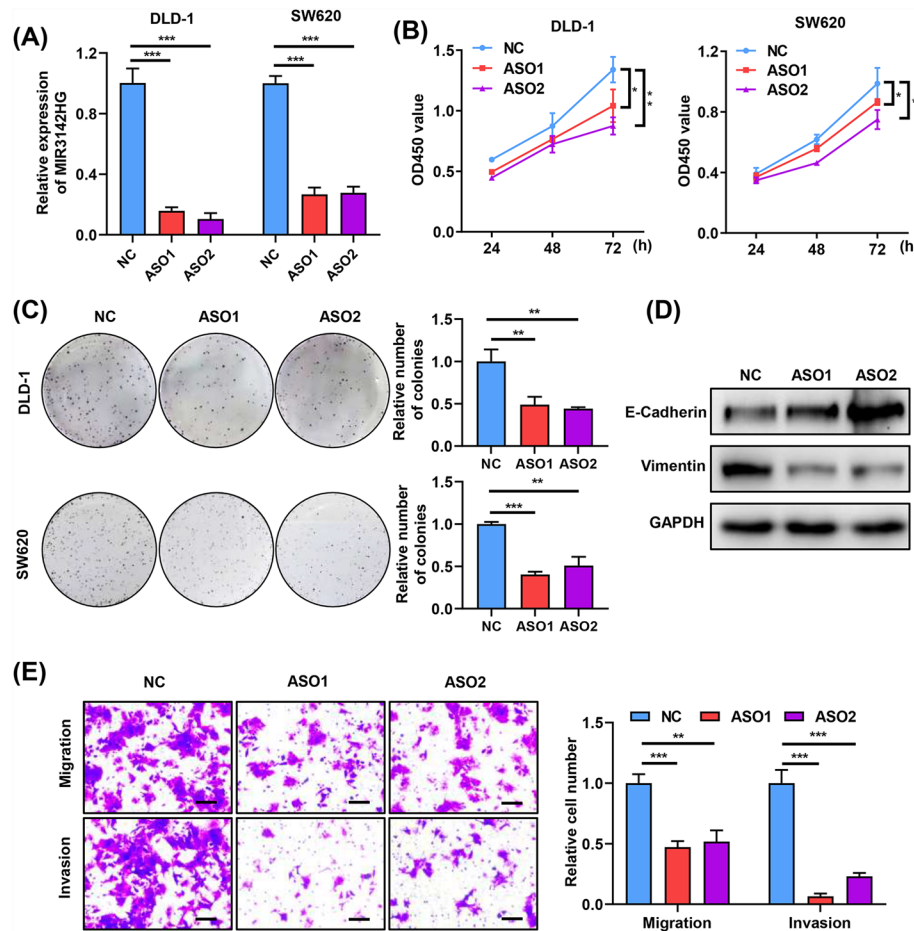
Fig. 3 MIR3142HG knockdown suppresses CRC cell proliferation, migration, and invasion in vitro. **A** qRT-PCR was used to assess the ASO-mediated knockdown efficiency of MIR3142HG in DLD-1 and SW620 cells transfected with NC-ASO, MIR3142HG-ASO1, or MIR3142HG-ASO2 for 48 h. **B**, **C** The proliferation ability of DLD-1 and SW620 cells transfected with NC-ASO, MIR3142HG-ASO1, or MIR3142HG-ASO2 was assessed by CCK-8 (**B**) and colony formation assays (**C**). **D** E-cadherin and vimentin protein expression in DLD-1 cells transfected with NC-ASO, MIR3142HG-ASO1, or MIR3142HG-ASO2 was detected by western blot analysis. **E** Migration and invasion abilities of DLD-1 cells transfected with NC-ASO, MIR3142HG-ASO1, or MIR3142HG-ASO2 were assessed via Transwell assays. Scale bar: 100 μm. Data represent the mean ± SD of three independent experiments. *$P < 0.05$, **$P < 0.01$, ***$P < 0.001$

MIR3142HG knockdown suppresses CRC cell proliferation, migration, and invasion in vitro

We designed two ASOs that specifically target human MIR3142HG sequences. The mRNA expression of MIR3142HG was significantly suppressed by transfection with MIR3142HG-ASOs in DLD-1 and SW620 cells (Fig. 3A). MIR3142HG knockdown by ASOs significantly inhibited cell growth, as shown by CCK-8 and plate colony formation assays (Fig. 3B, C), and suppressed EMT (E-cadherin protein expression increased and vimentin protein expression decreased) and the migration and invasion of CRC cells (Fig. 3D, E).

MIR3142HG knockdown suppresses the growth of CRC in patient-derived organoids and xenograft mouse models

In addition, patient-derived organoids of patients with CRC treated with MIR3142HG-ASOs presented a significant reduction in the number and volume of spheres (Fig. 4A) and inhibited organoid growth by quantitating ATP production (Fig. 4B). Moreover,
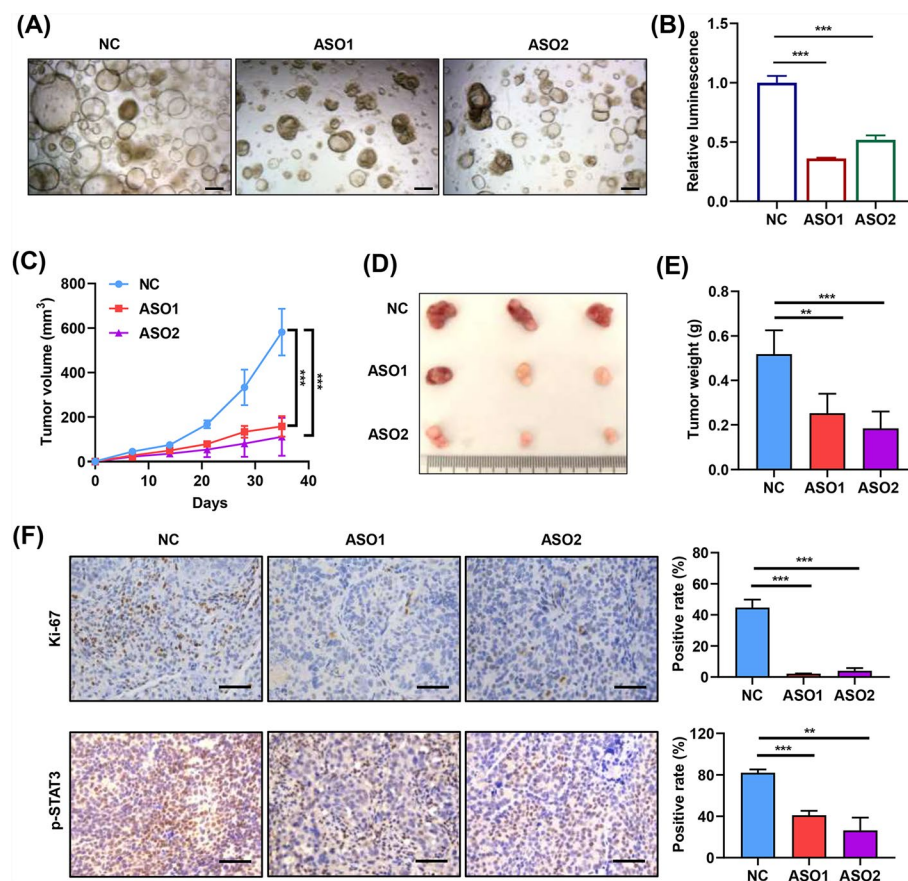

Fig. 4 MIR3142HG knockdown suppresses the growth of CRC in patient-derived organoids and xenograft mouse models. **A** Brightfield images of patient-derived organoids of patients with colorectal cancer treated with Negative control (NC) or MIR3142HG-ASOs for 5 days. Scale bar: 200 μm. **B** The growth of patient-derived organoids was assessed via adenosine triphosphate (ATP) detection ($n = 3$). Organoids were treated with NC or MIR3142HG-ASOs for 5 days. **C** Tumor volumes from different groups were measured every week ($n = 5$). **D** Representative photographs of excised xenograft tumors. **E** The tumor weights of all the groups were measured ($n = 5$). **F** Ki-67 and p-STAT3 protein expression in xenograft tumor tissues was assessed by immunostaining. Scale bar: 100 μm. Data represent the mean $\pm$ SD. **$P < 0.01$, ***$P < 0.001$

treatment with MIR3142HG-ASOs significantly suppressed tumor growth in nude mice (Fig. 4C–E) and decreased the expression of Ki-67 and p-STAT3 in tumor tissues (Fig. 4F).

The transcriptional regulation of MIR3142HG expression by the IL-6/STAT3 pathway

We performed qRT-PCR analysis to determine whether STAT3 affects the expression of MIR3142HG. As expected, IL-6-induced MIR3142HG expression was partially reversed by silencing STAT3 (Fig. 5A). The inhibition of STAT3 activity by S3I-201 also resulted in the suppression of MIR3142HG expression (Fig. 5B). To confirm that MIR3142HG is a STAT3 transcriptional target, a pGL3-basic vector was used to clone serial truncations of the MIR3142HG gene promoter, and luciferase activity was measured after the transfection of these constructs into HEK-293 T cells. The results showed that high transcriptional activity was correlated with approximately −1000 to −500 nt
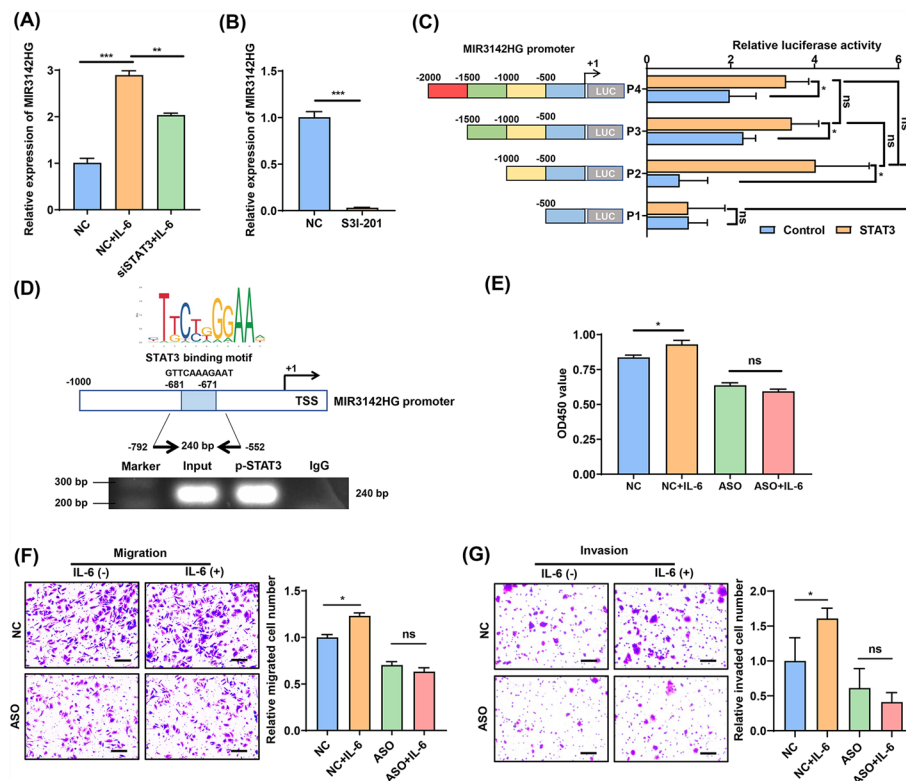

Fig. 5 The transcriptional regulation of MIR3142HG expression by the IL-6/STAT3 pathway. **A** qRT-PCR analysis of MIR3142HG expression in SW480 cells transfected with NC or STAT3 siRNA and treated with IL-6 for 24 h. **B** qRT-PCR analysis of MIR3142HG expression in SW480 cells with or without S3I-201 treatment. **C** Deletion map of the STAT3-binding domain in the MIR3142HG promoter. Left: diagrams of the upstream domain of the MIR3142HG promoter and the truncated fragments. Right: luciferase assays were performed using HEK-293 T cells transfected with the indicated vectors. **D** Potential STAT3 binding sites on the MIR3142HG gene promoter were predicted via JASPAR (upper panel). ChIP analysis of STAT3 enrichment at the MIR3142HG promoter in SW480 cells (lower panel). **E** The proliferation ability of SW480 cells transfected with MIR3142HG-ASO or NC-ASO and treated with IL-6 was assessed via a CCK-8 assay. **F**, **G** Migration and invasion abilities of SW480 cells transfected with MIR3142HG-ASO or NC-ASO and treated with IL-6 were assessed via Transwell assays. Scale bar: 100 μm. Data represent the mean ± SD of three independent experiments. *ns* not significant, *$P < 0.05$, **$P < 0.01$, ***$P < 0.001$

of the promoter region (Fig. 5C), suggesting that this region contains a regulatory element critical for the transcription of MIR3142HG. The high-quality transcription factor binding profile database JASPER predicted four potential binding regions of STAT3 on the MIR3142HG promoter. We observed enrichment of the MIR3142HG promoter fragment with an anti-p-STAT3 antibody via a ChIP assay (Fig. 5D). CCK-8 and Transwell assays were used to observe the growth, migration, and invasion of SW480 cells transfected with MIR3142HG-ASO after treatment with IL-6. We found that the knockdown of MIR3142HG completely blocked the IL-6-induced increase in cell proliferation, migration, and invasion (Fig. 5E–G).

MIR3142HG increases STAT3 phosphorylation by interacting with STAT3 and Trx-1

We further investigated whether MIR3142HG affects STAT3 activation in CRC cells. After MIR3142HG was knocked down by ASOs in SW480 cells, western blotting revealed that the protein expression of p-STAT3 and Trx-1 decreased significantly (Fig. 6A), but the mRNA expression of Trx-1 and STAT3 was not affected (Fig. 6B). We hypothesized that the effect of MIR3142HG on STAT3 and Trx-1 does not occur at the transcriptional level. Co-immunoprecipitation (co-IP) analysis showed that overexpression of MIR3142HG increased the interaction between Trx-1 and STAT3 in SW480 cells, whereas knockdown of MIR3142HG decreased the interaction between Trx-1
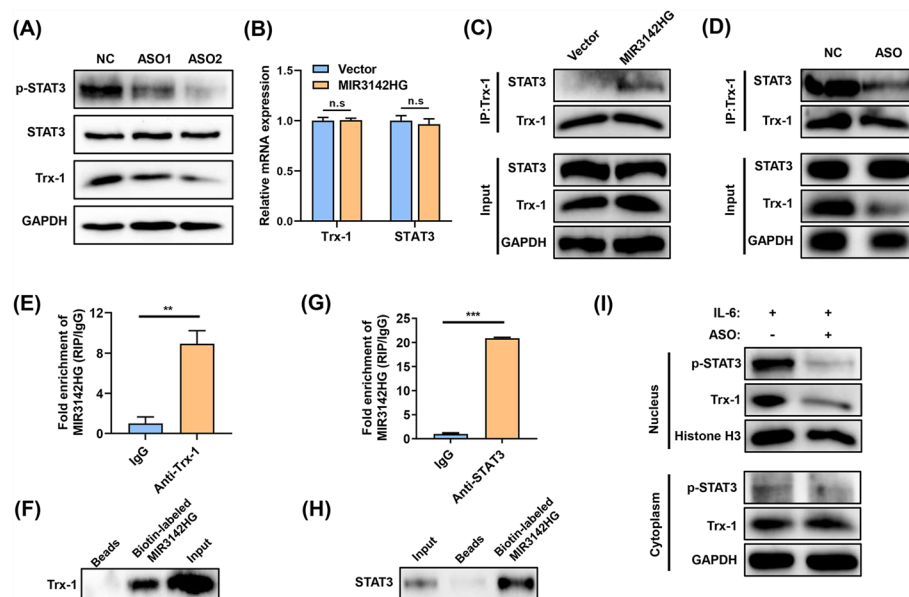

Fig. 6 MIR3142HG increases STAT3 phosphorylation by interacting with STAT3 and Trx-1. **A** Western blot analysis of Trx-1, STAT3, and p-STAT3 protein expression in SW480 cells transfected with NC or MIR3142HG-ASOs. **B** qRT-PCR analysis of Trx-1 and STAT3 mRNA expression in SW480 cells transfected with NC or MIR3142HG-ASOs. **C** Co-IP analysis of the interaction between Trx-1 and STAT3 in SW480 cells transfected with the control vector or MIR3142HG vector. **D** Co-IP analysis of the interaction between Trx-1 and STAT3 in SW480 cells transfected with NC or MIR3142HG-ASO. **E**, **F** RIP (**E**) and RNA pulldown assays (**F**) were performed to determine the interaction between MIR3142HG and Trx-1. **G**, **H** RIP (**G**) and RNA pulldown assays (**H**) were performed to determine the interaction between MIR3142HG and STAT3. **I** Western blot analysis of Trx-1 and p-STAT3 protein expression in the nucleus and cytoplasm of SW480 cells transfected with NC or MIR3142HG-ASO under IL-6 treatment. Data represent the mean ± SD of three independent experiments. **P < 0.01, ***P < 0.001

and STAT3 (Fig. 6C, D). Both RIP and RNA pulldown assays revealed that MIG3142HG specifically interacted with endogenous STAT3 and Trx-1 (Fig. 6E–H). Moreover, MIR3142HG knockdown by ASO apparently decreased the expression of p-STAT3 and Trx-1 in the nucleus upon treatment with IL-6 (Fig. 6I). These results suggest that MIR3142HG may increase the nuclear translocation of the Trx-1/STAT3 complex in CRC cells by interacting with STAT3 and Trx-1, thereby promoting STAT3 activation.

MIR3142HG serves as a potential diagnostic and predictive biomarker for the dual characteristics of CRC progression

To investigate the expression patterns of MIR3142HG in CRC tissues, data from the Cancer Genome Atlas (TCGA) database were analyzed. The result revealed that MIR3142HG was aberrantly expressed in CRC tissues compared with normal tissues (Fig. 7A). A GEPIA2 web tool analysis also showed that both colon adenocarcinoma (COAD) and rectum adenocarcinoma (READ) tissues had higher MIR3142HG expression than normal tissues did (Fig. 7B). However, low MIR3142HG expression was significantly associated with advanced tumor, node, metastasis (TNM) stages in patients with CRC (Fig. 7C). Moreover, in the TCGA dataset, higher MIR3142HG expression was associated with better overall survival (OS) but was not significantly related to disease-free survival (DFS) (Fig. 7D, E). We also detected the expression of MIR3142HG in tissue microarrays with 443 CRC tissues and 59 normal tissues by ISH assay. We were unable to determine the expression of MIR3142HG in paracancerous tissues. However, the expression of MIR3142HG was easily detected in most CRC tissues, indicating that MIR3142HG was significantly upregulated in our cohort of CRC samples (Fig. 7F, G). ROC analysis revealed that MIR3142HG expression was a good predictor of CRC (area under the curve (AUC) $= 0.8070$; Fig. 7H). Consistent with the results of the TCGA database analysis, low MIR3142HG expression was significantly associated with advanced stage and unfavorable survival in patients with CRC (Fig. 7I–N, Supplementary Material Tables S4–S6).

Discussion

IL-6 is a typical inflammatory cytokine that is overexpressed in a variety of tumors, including CRC. IL-6 signaling leads to numerous malignant processes in neoplastic cells via continuous activation of STAT3, including cell cycle progression, proliferation, antiapoptosis, invasion and metastasis, EMT, angiogenesis, and drug resistance [25], and plays a critical role in the development of CRC [26]. STAT3, an important transcription factor, can modulate the transcription of numerous downstream genes, including lncRNAs [27]. There is growing evidence that lncRNAs are closely associated with tumorigenesis, progression, prognosis, and drug resistance [28]. LncRNAs not only have multiple biological functions, including regulation of the cell cycle, cell differentiation and cell apoptosis [29, 30], but also play a role as tumor-promoting or tumor-suppressing factors; independently, they can influence the proliferation and metastasis of cancer cells [31].

Our previous studies have shown that the nuclear translocation of Trx-1 promotes CRC progression by enhancing IL-6/STAT3 signaling through interaction with STAT3 [21]. In this study, we performed RNA-Seq in wild-type and Trx-1-knockdown SW480
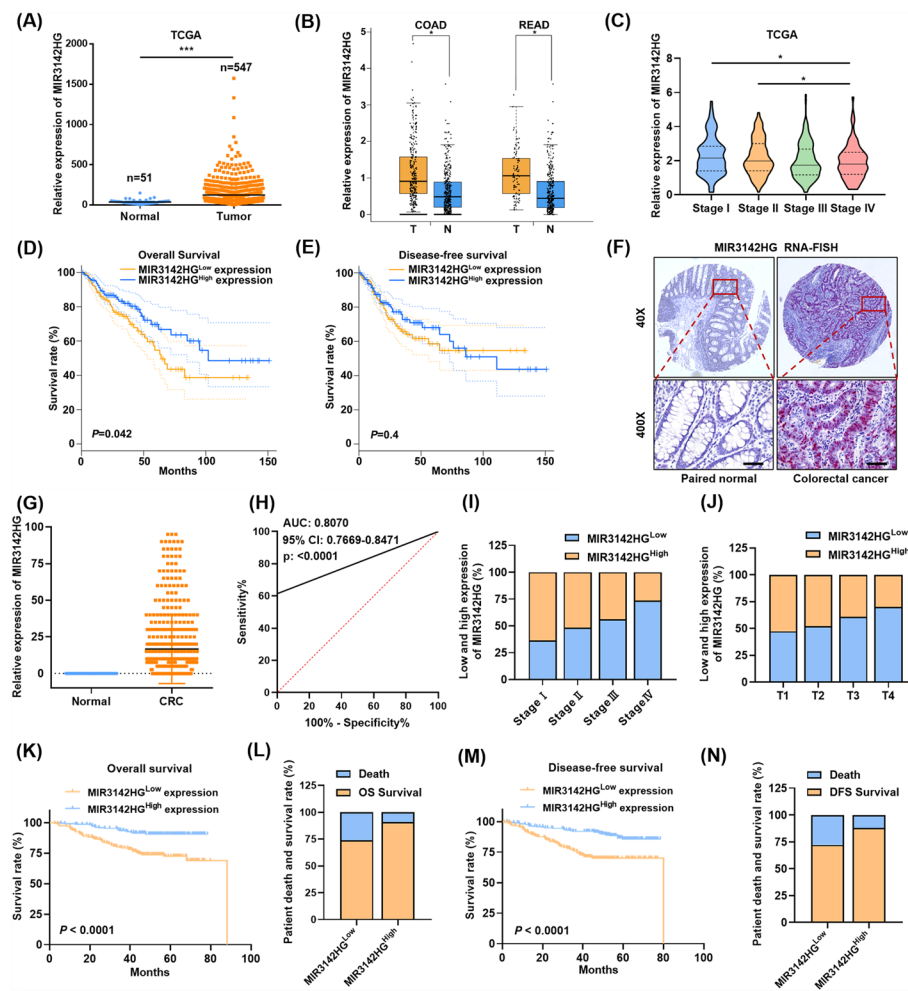
Fig. 7 MIR3142HG serves as a potential diagnostic and predictive biomarker for the dual characteristics of CRC progression. **A** Comparison of the expression of MIR3142HG in adjacent normal tissue (*n* = 51) and CRC tissue (*n* = 647) from the TCGA database. **B** Expression of MIR3142HG in colon and rectum samples compared with adjacent normal samples via the GEPIA2 web tool (http://gepia2.cancer-pku.cn/). **C** Violins showing MIR3142HG expression in different stages of CRC according to the TCGA database. **D**, **E** Kaplan–Meier curves estimating overall survival and disease-free survival according to the patients divided into low and high MIR3142HG expression groups in the TCGA dataset cohort. **F**, **G** ISH was performed to determine MIR3142HG expression in CRC tissues and adjacent noncancerous tissues. Scale bar: 100 μm. **H** Receiver operating characteristic (ROC) curves for MIR3142HG expression as a potential biomarker in CRC. **I**, **J** Proportion of samples with high MIR3142HG staining intensity and low MIR3142HG staining intensity at different stages. **K–N** Kaplan–Meier survival curves for overall survival (OS) and disease-free survival (DFS) according to patient division into low and high MIR3142HG expression levels in our pathological microarray cohort. The data represent mean ± SD. *$P < 0.05$, ***$P < 0.001$

cells treated with IL-6. We found that the expression of MIR3142HG was upregulated by IL-6 in CRC cells and that knockdown of Trx-1 or inhibition of STAT3 partially blocked this induction by IL-6. Further studies revealed that STAT3, as a transcription factor, has the ability to bind to the MIR3142HG promoter region and stimulate the transcriptional activity of MIR3142HG.

MIR3142HG is located at human chromosome 5q33.3, also known as the the host gene for miR-3142 and miR-146a [32]. Previous studies have shown that MIR3142HG is involved in lipopolysaccharide-induced acute lung injury and idiopathic pulmonary

fibrosis by affecting the inflammatory response [33, 34]. MIR3142HG single-nucleotide polymorphisms have been reported to be significantly associated with the risk of IgA nephropathy [35], osteonecrosis of the femoral head [36], lumbar disc herniation [37], and glioma [32]. However, few studies have investigated the function of MIR3142HG in cancer. In this study, we found that MIR3142HG expression was induced by IL-6 in CRC cells. MIR3142HG knockdown reversed IL-6-induced CRC cell proliferation and migration. MIR3142HG overexpression promoted CRC cell proliferation, migration, and invasion. Conversely, the knockdown of MIR3142HG by ASOs suppressed CRC cell proliferation, migration, and invasion in vitro, as well as the growth of tumors in patient-derived organoids and xenograft mouse models. These results suggest that MIR3142HG plays a key role in the development of CRC and may be a therapeutic target. In vitro and in vivo experiments validated the therapeutic efficacy of ASOs targeting MIR3142HG, suggesting that the strategy of targeting MIR3142HG has potential clinical value.

MIR3142HG is the host gene that encodes two miRNAs: miR-146a and miR-3142. MiR-146a is frequently downregulated in CRC tissues and functions as a tumor suppressor by targeting oncogenic pathways [38–41]. These functions are in exact contradiction to the phenotypes of MIR3142HG observed in our study. The second miRNA, miR-3142 is less well-characterized, and its functional relevance in CRC remains unexplored. Studies have reported that circTAB2 can act as a ceRNA and directly interact with miR-3142, thereby regulating GLIS2/AKT to inhibit tumorigenesis in lung cancer [42]. Our study primarily focused on the MIR3142HG transcript as a functional lncRNA and did not directly test whether MIR3142HG regulates the miRNAs it harbors. Our study identified MIR3142HG, which could promote CRC progression by interacting with STAT3 and Trx-1. MIR3142HG knockdown by ASOs decreased the protein expression of p-STAT3 and Trx-1 and suppressed the interaction between Trx-1 and STAT3. However, overexpression of MIR3142HG increased the interaction between Trx-1 and STAT3 in SW480 cells. RIP and RNA pulldown assays revealed that MIG3142HG specifically interacted with endogenous STAT3 and Trx-1. The activity of transcription factors is often activated by interactions with lncRNAs [9]. Chen and colleagues reported that lncSox4 directly interacts with STAT3 and recruits it to the Sox4 promoter to initiate its transcription [43]. In addition, a previous study showed that PVT1 physically interacts with STAT3 in the nucleus, thereby preventing the polyubiquitylation of STAT3 and subsequent proteasome-mediated degradation [44]. In our study, we demonstrated that MIR3142HG can interact with STAT3 and Trx-1. This interaction may stabilize STAT3 and Trx-1 by enhancing their combination and increasing their nuclear expression. These results suggest that MIR3142HG may activate IL-6/STAT3 signaling and promote CRC progression by interacting with STAT3 and Trx-1.

Many lncRNAs exhibit tissue-specific and subsequent cancer-specific expression patterns, which are necessary as tumor biomarkers [45, 46]. A growing number of studies have shown that lncRNAs can be used as potential biomarkers for cancer [47, 48]. Owing to the critical role of MIR3142HG in CRC development, we analyzed its expression in tumor tissues via both the TCGA database and our pathological paraffin microarray analysis. The results revealed significant upregulation of MIR3142HG in CRC tissues compared with the corresponding adjacent regions. In normal adjacent tissues, the expression of MIR3142HG is almost undetectable by ISH. We hypothesized that

MIR3142HG is active at the time of tumor formation. MIR3142HG detected in pathological samples may indicate the presence of CRC tumors. We then examined the relationship between MIR3142HG expression and pathological stage. To our surprise, low expression of MIR3142HG in CRC tissues was associated with advanced stage disease. The activity of lncRNAs is often highly context-dependent, influenced by tumor stage, microenvironment, or coexisting mutations. While MIR3142HG promotes migration and invasion in vitro, its downregulation in advanced stages in vivo may reflect a shift in its functional role or regulatory interactions at later stages. For example, MIR3142HG might drive early metastatic events (e.g., epithelial-to-mesenchymal transition); however, its sustained expression could become detrimental to survival in disseminated or immune-exposed microenvironments, leading to negative selection in advanced tumors. However, we still need more experiments to resolve this paradox. Our findings suggest that the aberrant expression of MIR3142HG plays a more important role in the early stage of tumor formation. Since the patients with high expression of MIR3142HG were mostly at an early tumor stage, it can be assumed that they generally had a better prognosis after aggressive surgery. Our prognostic analysis also confirmed that high MIR3142HG expression was correlated with longer survival in patients with CRC. Although the presence of MIR3142HG is indicative of tumorigenesis, high MIR3142HG expression is a favorable predictor of cancer prognosis in terms of OS, DFS, and clinical stage.

Conclusions

We identified a novel IL-6-induced lncRNA, MIR3142HG, that promotes CRC progression by activating the IL-6/STAT3 signaling pathway through interactions with STAT3 and Trx-1. In addition, MIR3142HG is highly expressed in CRC tissues, and its expression is associated with the prognosis of patients with CRC. Our findings uncover the role of MIR3142HG in IL-6-induced CRC growth and metastasis, which represents a potential new target for diagnosing and treating CRC.

Abbreviations
CRC   Colorectal cancer
LncRNAs   Long noncoding RNAs
STAT3   Signal transducer and activator of transcription 3
Trx-1   Thioredoxin-1
ASO   Antisense oligonucleotide
RIP   RNA-binding protein immunoprecipitation
RNA-FISH   RNA fluorescence in situ hybridization
TCGA   The Cancer Genome Atlas

Supplementary Information

The online version contains supplementary material available at https://doi.org/10.1186/s11658-025-00742-6.

Supplementary material 1.

Declarations

Ethics approval and consent to participate

Colorectal cancer tissues were obtained by surgery with the written consent of patients who underwent surgery at the First Affiliated Hospital of Wenzhou Medical University, and the study was authorized by the Ethics Committee of the First Affiliated Hospital of Wenzhou Medical University in accordance with the provisions of the Helsinki Declaration (approval no. KY2022-R101; date: 20 June 2022). The in vivo animal experiment was approved by the Laboratory Animal Ethics Committee of the First Affiliated Hospital of Wenzhou Medical University (approval no. WYYY-AEC-2021-305; 21 December 2021) and was conducted in compliance with the International Council for Laboratory Animal Science (ICLAS) guidelines (governing board approval: 6 June 2013).

Consent for publication

All authors agreed to publish this manuscript.

Competing interests

The authors declare that they have no known competing financial interests or personal relationships that could have appeared to influence the work reported in this paper.

References

1. Bray F, Ferlay J, Soerjomataram I, Siegel RL, Torre LA, Jemal A. Global cancer statistics 2018: GLOBOCAN estimates of incidence and mortality worldwide for 36 cancers in 185 countries. CA Cancer J Clin. 2018;68(6):394–424.
2. Eng C, Yoshino T, Ruiz-Garcia E, Mostafa N, Cann CG, O'Brian B, et al. Colorectal cancer. Lancet. 2024;404(10449):294–310.
3. Wang L, Choi HS, Su Y, Lee B, Song JJ, Jang YS, et al. 7S,15R-dihydroxy-16S,17S-epoxy-docosapentaenoic acid, a novel DHA epoxy derivative, inhibits colorectal cancer stemness through repolarization of tumor-associated macrophage functions and the ROS/STAT3 signaling pathway. Antioxidants. 2021;10(9):1459.
4. Coussens LM, Werb Z. Inflammation and cancer. Nature. 2002;420(6917):860–7.
5. Soler MF, Abaurrea A, Azcoaga P, Araujo AM, Caffarel MM. New perspectives in cancer immunotherapy: targeting IL-6 cytokine family. J Immunother Cancer. 2023;11(11): e007530.
6. Tsai SC, Wu WC, Yang JS. Tetrandrine inhibits epithelial-mesenchymal transition in IL-6-Induced HCT116 human colorectal cancer cells. Onco Targets Ther. 2021;14:4523–36.
7. Guo JH, Thuong LHH, Jiang YJ, Huang CL, Huang YW, Cheng FJ, et al. Cigarette smoke promotes IL-6-dependent lung cancer migration and osteolytic bone metastasis. Int J Biol Sci. 2024;20(9):3257–68.
8. Jones SA, Jenkins BJ. Recent insights into targeting the IL-6 cytokine family in inflammatory diseases and cancer. Nat Rev Immunol. 2018;18(12):773–89.
9. Long Y, Wang X, Youmans DT, Cech TR. How do lncRNAs regulate transcription? Sci Adv. 2017;3(9):eaao2110.
10. Grivennikov S, Karin E, Terzic J, Mucida D, Yu GY, Vallabhapurapu S, et al. IL-6 and Stat3 are required for survival of intestinal epithelial cells and development of colitis-associated cancer. Cancer Cell. 2009;15(2):103–13.
11. Waldner MJ, Foersch S, Neurath MF. Interleukin-6—A key regulator of colorectal cancer development. Int J Biol Sci. 2012;8(9):1248–53.
12. Anderson DM, Anderson KM, Chang CL, Makarewich CA, Nelson BR, McAnally JR, et al. A micropeptide encoded by a putative long noncoding RNA regulates muscle performance. Cell. 2015;160(4):595–606.
13. Ahmad M, Weiswald LB, Poulain L, Denoyelle C, Meryet-Figuiere M. Involvement of lncRNAs in cancer cells migration, invasion and metastasis: cytoskeleton and ECM crosstalk. J Exp Clin Cancer Res. 2023;42(1):173.
14. Nyati KK, Hashimoto S, Singh SK, Tekguc M, Metwally H, Liu YC, et al. The novel long noncoding RNA AU021063, induced by IL-6/Arid5a signaling, exacerbates breast cancer invasion and metastasis by stabilizing Trib3 and activating the Mek/Erk pathway. Cancer Lett. 2021;520:295–306.
15. Su K, Zhao Q, Bian A, Wang C, Cai Y, Zhang Y. A novel positive feedback regulation between long noncoding RNA UICC and IL-6/STAT3 signaling promotes cervical cancer progression. Am J Cancer Res. 2018;8(7):1176–89.
16. Wu S, Liu B, Zhang Y, Hong R, Liu S, Xiang T, et al. Long non-coding RNA LEISA promotes progression of lung adenocarcinoma via enhancing interaction between STAT3 and IL-6 promoter. Oncogene. 2021;40(19):3449–59.
17. Ma Y, Zhu Y, Shang L, Qiu Y, Shen N, Wang J, et al. LncRNA XIST regulates breast cancer stem cells by activating proinflammatory IL-6/STAT3 signaling. Oncogene. 2023;42(18):1419–37.
18. Muri J, Kopf M. The thioredoxin system: balancing redox responses in immune cells and tumors. Eur J Immunol. 2023;53(1): e2249948.

19. Zhang J, Li X, Han X, Liu R, Fang J. Targeting the thioredoxin system for cancer therapy. Trends Pharmacol Sci. 2017;38(9):794–808.
20. Abdullah NA, Md Hashim NF, Muhamad Zakuan N, Chua JX. Thioredoxin system in colorectal cancer: its role in carcinogenesis, disease progression, and response to treatment. Life Sci. 2024;348:122711.
21. Wu A, Fang D, Liu Y, Shi X, Zhong Z, Zhou B, et al. Nuclear translocation of thioredoxin-1 promotes colorectal cancer development via modulation of the IL-6/STAT3 signaling axis through interaction with STAT3. Theranostics. 2023;13(14):4730–44.
22. Lin F, Zhang P, Zuo Z, Wang F, Bi R, Shang W, et al. Thioredoxin-1 promotes colorectal cancer invasion and metastasis through crosstalk with S100P. Cancer Lett. 2017;401:1–10.
23. Xie Y, Zheng ZW, He HT, Chang ZB. LncRNA NEAT1 induces autophagy through the miR-128-3p/ADAM28 axis to suppress apoptosis of non-small-cell lung cancer. Kaohsiung J Med Sci. 2022;38(10):933–49.
24. Pang Y, Wu J, Li X, Wang C, Wang M, Liu J, et al. NEAT1/miR-124/STAT3 feedback loop promotes breast cancer progression. Int J Oncol. 2019;55(3):745–54.
25. Lin Y, He Z, Ye J, Liu Z, She X, Gao X, et al. Progress in understanding the IL-6/STAT3 pathway in colorectal cancer. Onco Targets Ther. 2020;13:13023–32.
26. Johnson DE, O'Keefe RA, Grandis JR. Targeting the IL-6/JAK/STAT3 signalling axis in cancer. Nat Rev Clin Oncol. 2018;15(4):234–48.
27. Liu S, Li W, Liang L, Zhou Y, Li Y. The regulatory relationship between transcription factor STAT3 and noncoding RNA. Cell Mol Biol Lett. 2024;29(1):4.
28. Schwarzmueller L, Bril O, Vermeulen L, Leveille N. Emerging role and therapeutic potential of lncRNAs in colorectal cancer. Cancers. 2020;12(12):3843.
29. He A, He S, Peng D, Zhan Y, Li Y, Chen Z, et al. Prognostic value of long non-coding RNA signatures in bladder cancer. Aging. 2019;11(16):6237–51.
30. Liu D, Shi X. Long non-coding RNA NKILA inhibits proliferation and migration of lung cancer via IL-11/STAT3 signaling. Int J Clin Exp Pathol. 2019;12(7):2595–603.
31. Ashrafizadeh M, Gholami MH, Mirzaei S, Zabolian A, Haddadi A, Farahani MV, et al. Dual relationship between long non-coding RNAs and STAT3 signaling in different cancers: new insight to proliferation and metastasis. Life Sci. 2021;270:119006.
32. Guo X, Zhang M, Li Q, Zhao J, Wang B, Wang J, et al. Evaluation of genetic variants in MIR3142HG in susceptibility to and prognosis of glioma. Am J Clin Oncol. 2020;43(1):1–8.
33. Hadjicharalambous MR, Roux BT, Feghali-Bostwick CA, Murray LA, Clarke DL, Lindsay MA. Long non-coding RNAs are central regulators of the IL-1beta-induced inflammatory response in normal and idiopathic pulmonary lung fibroblasts. Front Immunol. 2018;9:2906.
34. Gao Y, Li S, Dong R, Li X. Long noncoding RNA MIR3142HG accelerates lipopolysaccharide-induced acute lung injury via miR-95-5p/JAK2 axis. Hum Cell. 2022;35(3):856–70.
35. Cao Y, Wang R, Zhang H, Zhai P, Wei J. Genetic variants in MIR3142HG contribute to the predisposition of IgA nephropathy in a Chinese Han population. Pub Health Genom. 2022;25:1–11.
36. Wang T, Wu H, Sun M, Liu T, An F, Dong Q, et al. Association between genetic polymorphisms of MIR3142HG and the risk of steroid-induced osteonecrosis of the femoral head in the population of Northern China. Pub Health Genom. 2021;25:1–9.
37. Dong Q, Ren G, Hao D. Assessment of MIR3142HG genetic polymorphisms and the susceptibility of lumbar disc herniation in the Chinese population. Sci Rep. 2024;14(1):29542.
38. Farc O, Budisan L, Zaharie F, Taulean R, Valean D, Talvan E, et al. Expression and functional analysis of immuno-micro-RNAs mir-146a and mir-326 in colorectal cancer. Curr Issues Mol Biol. 2024;46(7):7065–85.
39. Afshar-Khamseh R, Javeri A, Taha MF. MiR-146a suppresses the expression of CXCR4 and alters survival, proliferation and migration rate in colorectal cancer cells. Tissue Cell. 2021;73:101654.
40. Garo LP, Ajay AK, Fujiwara M, Gabriely G, Raheja R, Kuhn C, et al. MicroRNA-146a limits tumorigenic inflammation in colorectal cancer. Nat Commun. 2021;12(1):2419.
41. Bleau AM, Redrado M, Nistal-Villan E, Villalba M, Exposito F, Redin E, et al. miR-146a targets c-met and abolishes colorectal cancer liver metastasis. Cancer Lett. 2018;414:257–67.
42. Man W, Cui Y, Li J, Li Y, Jin J, Jin Y, et al. circTAB2 inhibits lung cancer proliferation, migration and invasion by sponging miR-3142 to upregulate GLIS2. Apoptosis. 2023;28(3–4):471–84.
43. Chen ZZ, Huang L, Wu YH, Zhai WJ, Zhu PP, Gao YF. LncSox4 promotes the self-renewal of liver tumour-initiating cells through Stat3-mediated Sox4 expression. Nat Commun. 2016;7:12598.
44. Zhao J, Du P, Cui P, Qin Y, Hu C, Wu J, et al. LncRNA PVT1 promotes angiogenesis via activating the STAT3/VEGFA axis in gastric cancer. Oncogene. 2018;37(30):4094–109.
45. de Goede OM, Nachun DC, Ferraro NM, Gloudemans MJ, Rao AS, Smail C, et al. Population-scale tissue transcriptomics maps long non-coding RNAs to complex disease. Cell. 2021;184(10):2633-481 e9.
46. Prensner JR, Chinnaiyan AM. The emergence of lncRNAs in cancer biology. Cancer Discov. 2011;1(5):391–407.
47. Fu D, Shi Y, Liu JB, Wu TM, Jia CY, Yang HQ, et al. Targeting long non-coding RNA to therapeutically regulate gene expression in cancer. Mol Ther Nucleic Acids. 2020;21:712–24.
48. Coan M, Haefliger S, Ounzain S, Johnson R. Targeting and engineering long non-coding RNAs for cancer therapy. Nat Rev Genet. 2024;25(8):578–95.

Publisher's Note